Cell Host & Microbe, Volume *16*

Supplemental Information

Nef Proteins of Epidemic HIV-1 Group O Strains Antagonize Human Tetherin

Silvia F. Kluge, Katharina Mack, Shilpa S. Iyer, François M. Pujol, Anke Heigele, Gerald H. Learn, Shariq M. Usmani, Daniel Sauter, Simone Joas, Dominik Hotter, Frederic Bibollet-Ruche, Lindsey J. Plenderleith, Martine Peeters, Matthias Geyer, Paul M. Sharp, Oliver T. Fackler, Beatrice H. Hahn, and Frank Kirchhoff

Supplemental Information

Supplemental Figure Inventory

Figure S1 (related to Figure 1). Expression and function of contemporary HIV-1 O Nef proteins.

Figure S2 (related to Figure 2). Sequences and function of HIV-1 MRCA Nef proteins.

Figure S3 (related to Figure 3). Mapping of amino acid residues in human tetherin targeted by HIV-1 O Nefs.

Figure S4 (related to Figure 4). Mapping of residues in HIV-1 O Nefs involved in downmodulation of human tetherin.

Figure S5 (related to Figure 5). Effect of O Nefs on intracellular expression and anterograde transport of human tetherin.

Figure S6 (related to Figure 6). O-Nefs trap human tetherin in the TGN during anterograde transport.

Figure S7 (related to Figure 7). Functional relevance of downmodulation of human tetherin by O-Nefs.

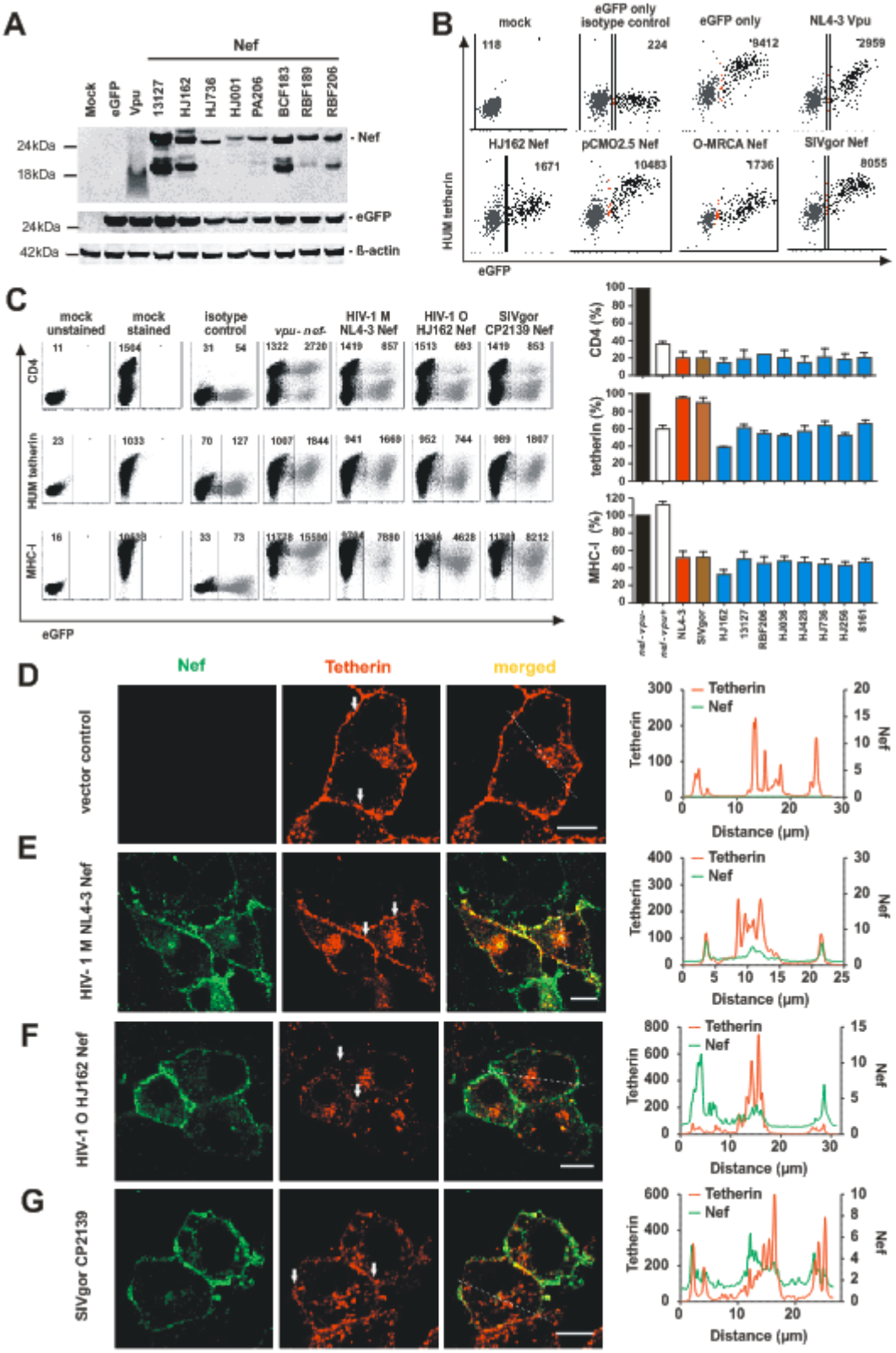
A
Nef
Mock
eGFP
Vpu
13127
HJ162
HJ736
HJ001
PA206
BCF183
RBF189
RBF206
24kDa
18kDa
- Nef
24kDa
- eGFP
42kDa
- ß-actin
B
mock
eGFP only isotype control
eGFP only
NL4-3 Vpu
118
224
9412
2959
HJ162 Nef
pCMO2.5 Nef
O-MRCA Nef
SIVgor Nef
1671
10483
1736
8055
HUM tetherin
eGFP
C
mock unstained
mock stained
isotype control
vpu- nef-
HIV-1 M NL4-3 Nef
HIV-1 O HJ162 Nef
SIVgor CP2139 Nef
CD4
HUM tetherin
MHC-I
eGFP
CD4 (%)
tetherin (%)
MHC-I (%)
nef- vpu-
nef- vpu+
NL4-3
SIVgor
HJ162
13127
RBF206
HJ036
HJ428
HJ736
HJ256
8161
D
E
F
G
Nef
Tetherin
merged
vector control
HIV- 1 M NL4-3 Nef
HIV-1 O HJ162 Nef
SIVgor CP2139
Tetherin
Nef
Distance (µm)

Figure S1 (related to Figure 1). Expression and function of contemporary HIV-1 O Nef proteins. (A) Expression of O-Nef proteins in 293T cells transfected with pCG constructs for the indicated *nef* alleles or an empty control vector. eGFP and ß-actin are shown as transfection and loading controls. (B) FACS analysis of 293T cells cotransfected with vectors expressing HUM tetherin and constructs expressing eGFP alone or together with the indicated *vpu* or *nef* alleles. The mean fluorescence intensities (MFIs) of HUM tetherin expression in transfected 293T cells are indicated. (C) FACS analysis (left) and quantification (right) of Nef-mediated modulation of CD4 and MHC-I on PBMCs transduced with vpu-defective HIV-1 NL4-3 IRES eGFP constructs expressing eGFP alone or together with the indicated *nef* alleles. eGFP expression levels used to calculate receptor expression and the mean fluorescence intensities (MFIs) are indicated. The right panel shows the levels of receptor expression in the presence of Nef relative to those measured in cells transfected with the GFP control vector (100%). Values are averages (±SEM) derived from three experiments. (D-G) Images show representative confocal acquisitions from 293T cells transfected with plasmids expressing HUM tetherin-HA and Nef-AU1 constructs. Shown are images of Nef (green) and tetherin (red) and merged images. Scale bars =10 μm. The regions utilized to generate the intensity profile plots are indicated by a line and the position of the membrane in the tetherin channel by arrows.

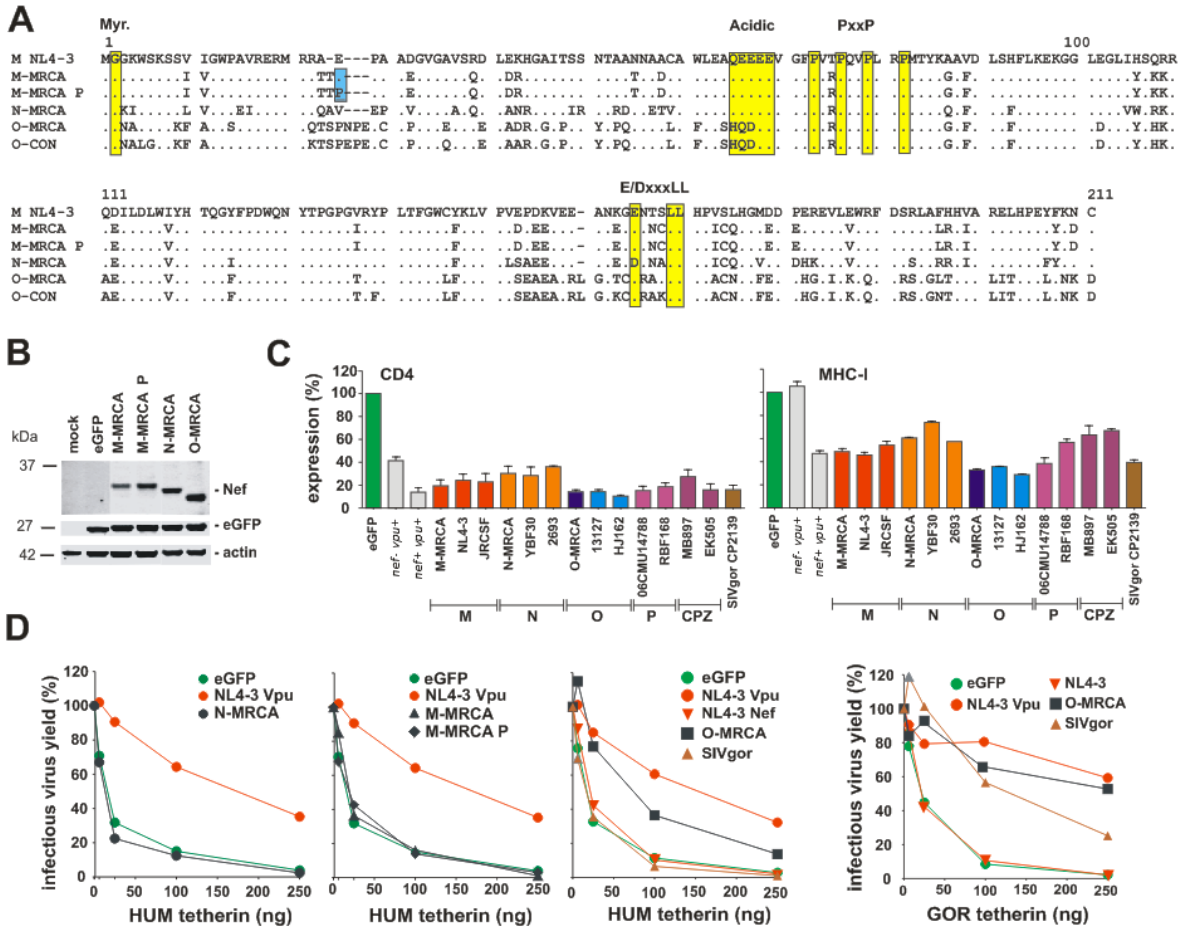

Figure S2 (related to Figure 2). Sequences and function of HIV-1 MRCA Nef proteins. (A) Alignment of Nef amino acid sequences of the MRCAs of HIV-1 M, N and O. The NL4-3 Nef is shown on top for comparison. The myristoylated N-terminus, the acidic region and the PxxP-motif, as well as the conserved core domain, the flexible C-loop region and the C-terminus in the NL4-3 Nef are indicated. Dashes indicate gaps introduced to optimize the alignment and the light blue bar the site where MRCA sequences could not be inferred unambiguously. (B) Expression of AU1-tagged MRCA Nef proteins. 293T cells were transfected with plasmids expressing the indicated *vpu* and *nef* alleles. Steady state expression levels were determined two days later by Western blot analysis. (C) Levels of CD4 and MHC-I cell surface expression in the presence of HIV-1 group M, N and O MRCA Vpu or Nef proteins relative to those measured in 293T cells transfected with the eGFP control vector (100%). Values in all panels are averages (±SEM) from at least three independent experiments. (D) Virus release from 293T cells following transfection with 4 µg of a Δ*vpu*/Δ*nef* proviral NL4-3 construct, 1 µg of Vpu or Nef expression constructs and varying amounts of plasmids expressing HUM or GOR (right panel) tetherin. Infectious virus was determined by infection of TZM-bl indicator cells and is shown as a percentage of that detected in the absence of tetherin (100%). All infections were performed in triplicate and the results were confirmed in independent experiments

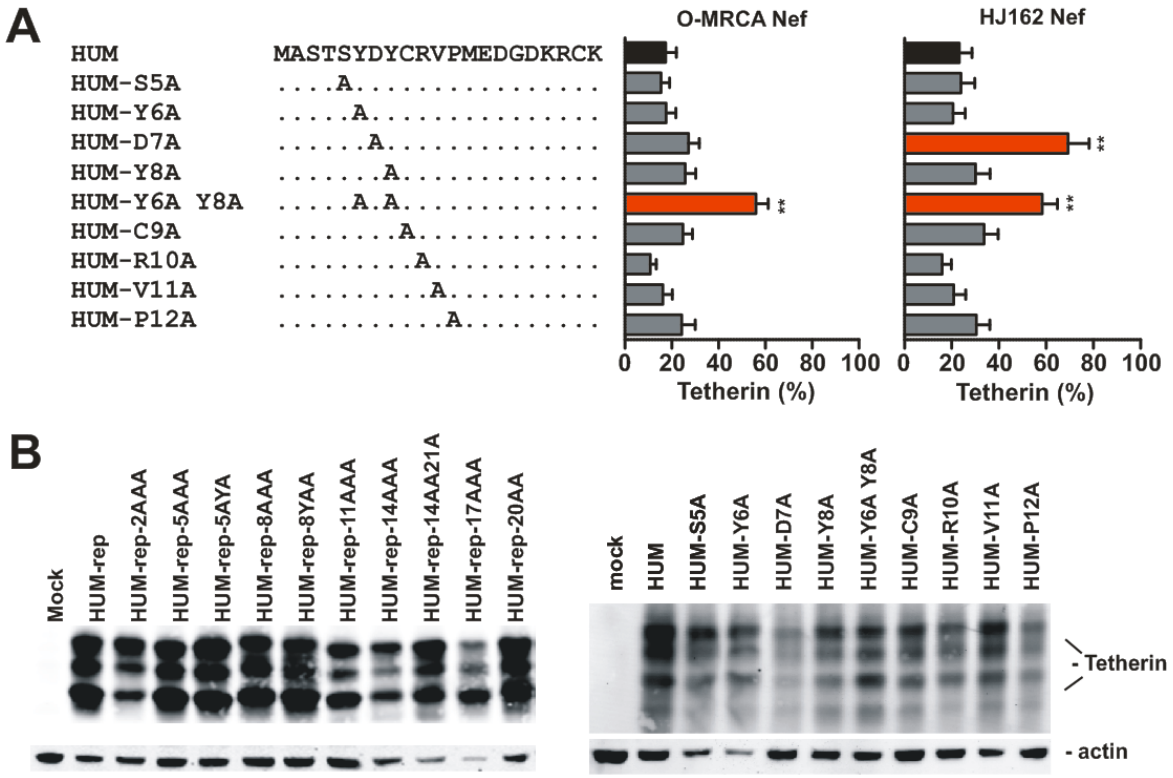

Figure S3 (related to Figure 3). Mapping of amino acid residues in human tetherin targeted by HIV-1 O Nefs. (A) Effect of alanine substitutions in the cytoplasmic part of HUM tetherin on susceptibility to O-MRCA and HJ162 *nef* alleles. Shown are the levels of tetherin cell surface expression in the presence of Nef relative to those measured in cells transfected with the GFP only control vector (100%). Shown are average values (±SEM) derived from three experiments. (B) Expression of tetherin variants containing mutations in their cytoplasmic domain. 293T cells were transfected with plasmids expressing the indicated mutant tetherin alleles. Steady state expression levels were determined two days later by Western blot analysis.

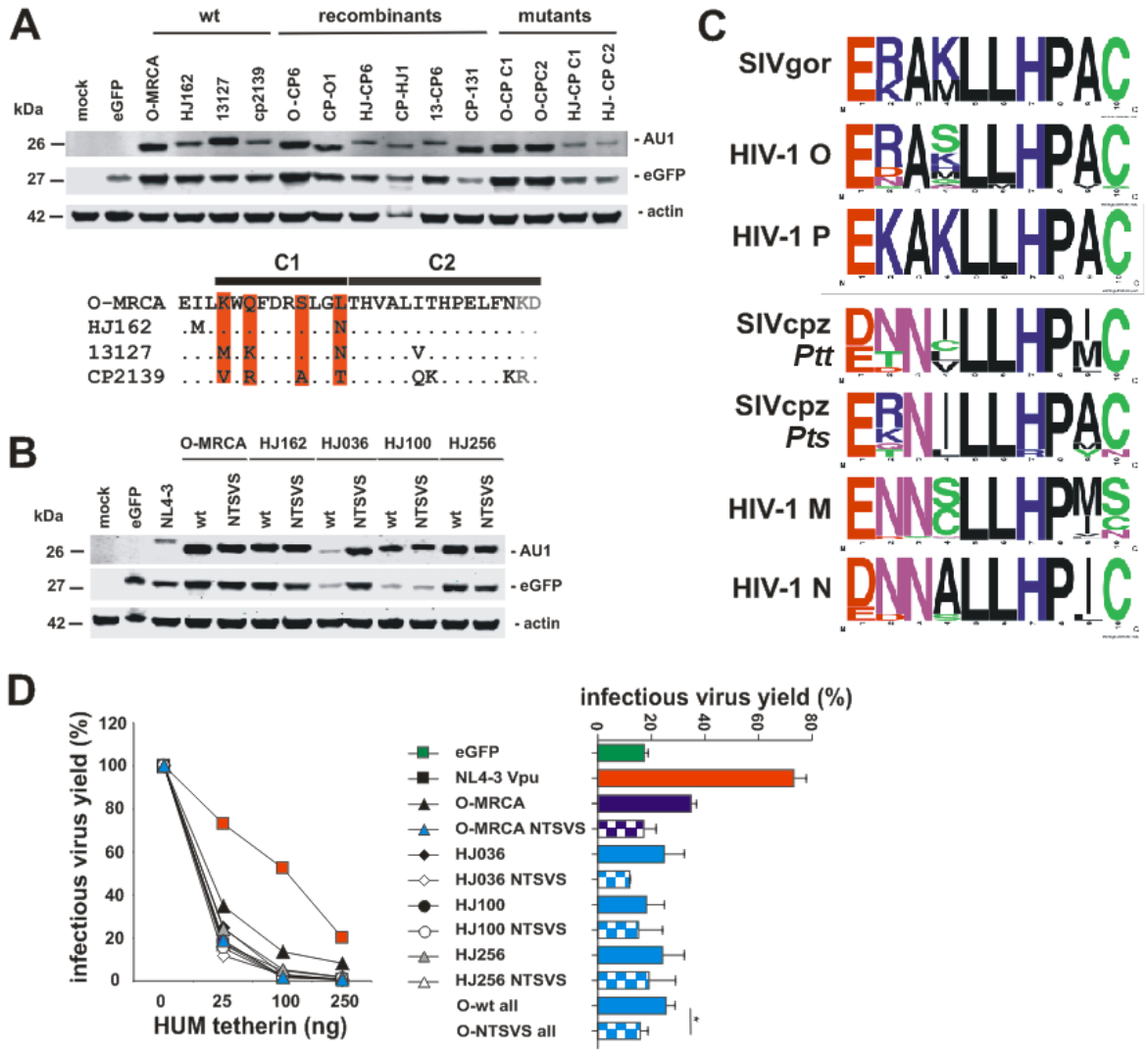

Figure S4 (related to Figure 4). Mapping of residues in HIV-1 O Nefs involved in downmodulation of human tetherin. (A, B) Expression of selected wt and mutant Nef proteins. 293T cells were transfected with expression plasmids encoding the indicated AU1-tagged Nefs and eGFP. Mock transfected cells were used as negative controls; ß-actin and eGFP expression levels were analyzed to control for loading and transfection efficiency, respectively. The alignment shows amino acid variations at the C-terminus of Nef proteins differing in the downmodulation capacity of HUM tetherin. Their localization in the structure of the HIV-1 Nef protein is shown in Figure 4C. (C) Frequency plots of amino acid residues in and near the putative D/ExxxLL interaction site of HIV-1 O, P, M and N and SIVcpz and SIVgor Nefs with adaptor protein complexes. (D) Effect of wild type and mutant O Nefs on infectious virus release. 293T cells were cotransfected with a Δ*vpu*Δ*nef* proviral HIV-1 NL4-3 construct, vectors expressing the indicated Nef proteins or Vpu and different quantities of constructs expressing HUM tetherin. The levels of infectious virus in the culture supernatant were determined by triplicate infection of TZM-bl cells as described in the methods section. The results show average values derived from two independent experiments and were confirmed by measuring the levels of p24 antigen in the cell culture supernatants. The right panel shows the average levels of infectious virus release (±SEM) in the presence of 25 ng of the HU-tetherin expression construct.

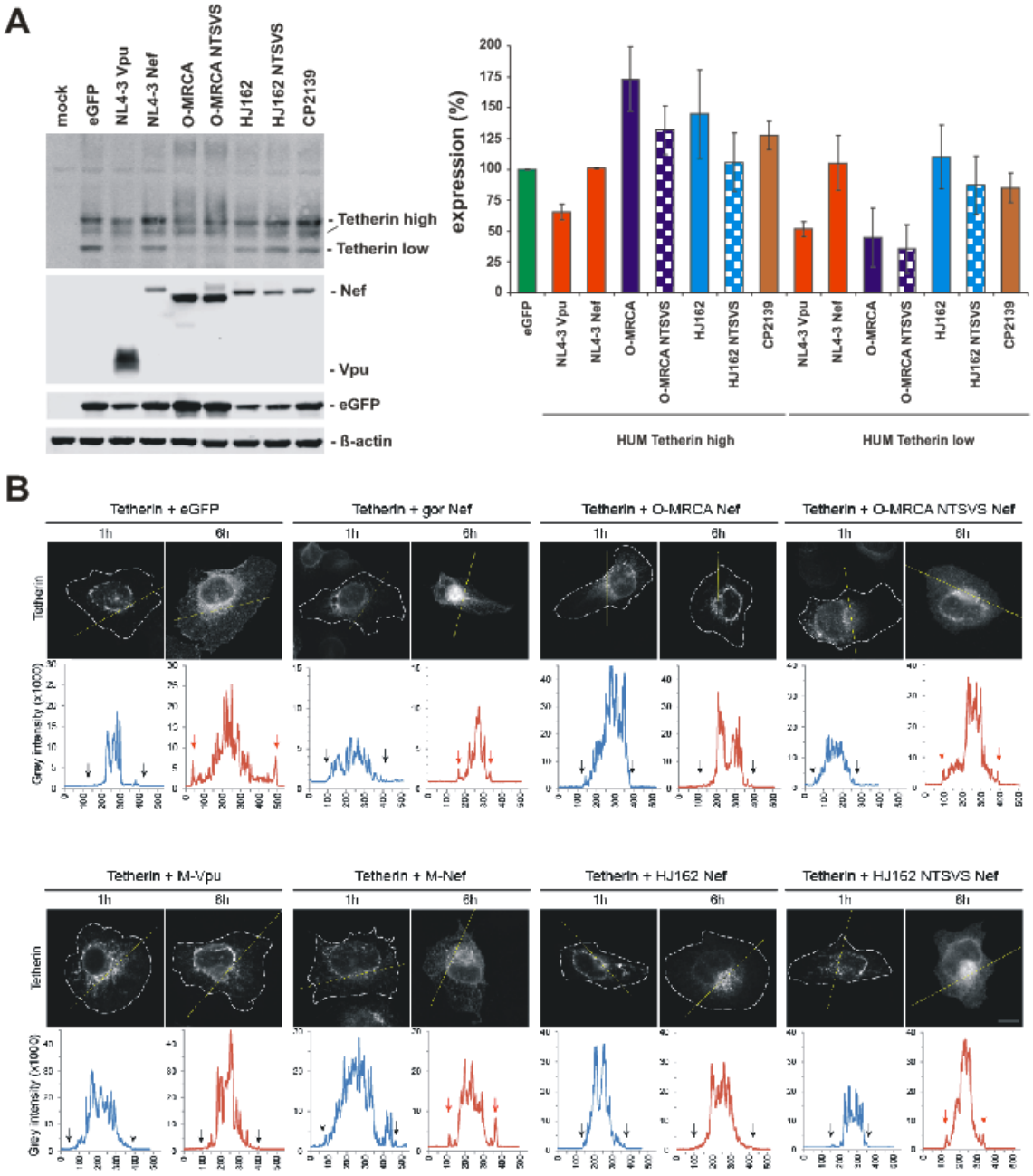

Figure S5 (related to Figure 5). Effect of O Nefs on intracellular expression and anterograde transport of human tetherin. (A) Human tetherin expression in the presence of Vpu or the indicated Nef proteins. 293T cells were cotransfected with plasmids expressing the indicated tetherin variants and Vpu or the indicated Nef proteins and examined by Western blot two days later. The right panel shows average levels (±SEM) of the intensities of the upper and lower tetherin signals in the presence or absence of Nef and Vpu. (B) Effect of O-Nefs on transport of newly synthesized HUM tetherin to the cell surface. The nuclei of HT1080 cells were co-microinjected with a HUM tetherin expression plasmid together with vectors encoding eGFP, or NL4-3 Vpu or the indicated Nef proteins. Microphotographs are representative of 200 microinjected cells. The lower panel provides the intensity blot of HUM tetherin cell expression at 1h or 6h post-microinjection, the arrows indicate the localization of the cellular membrane. Cell circumferences are indicated by white dashed lines. Scale bar = 10µM.

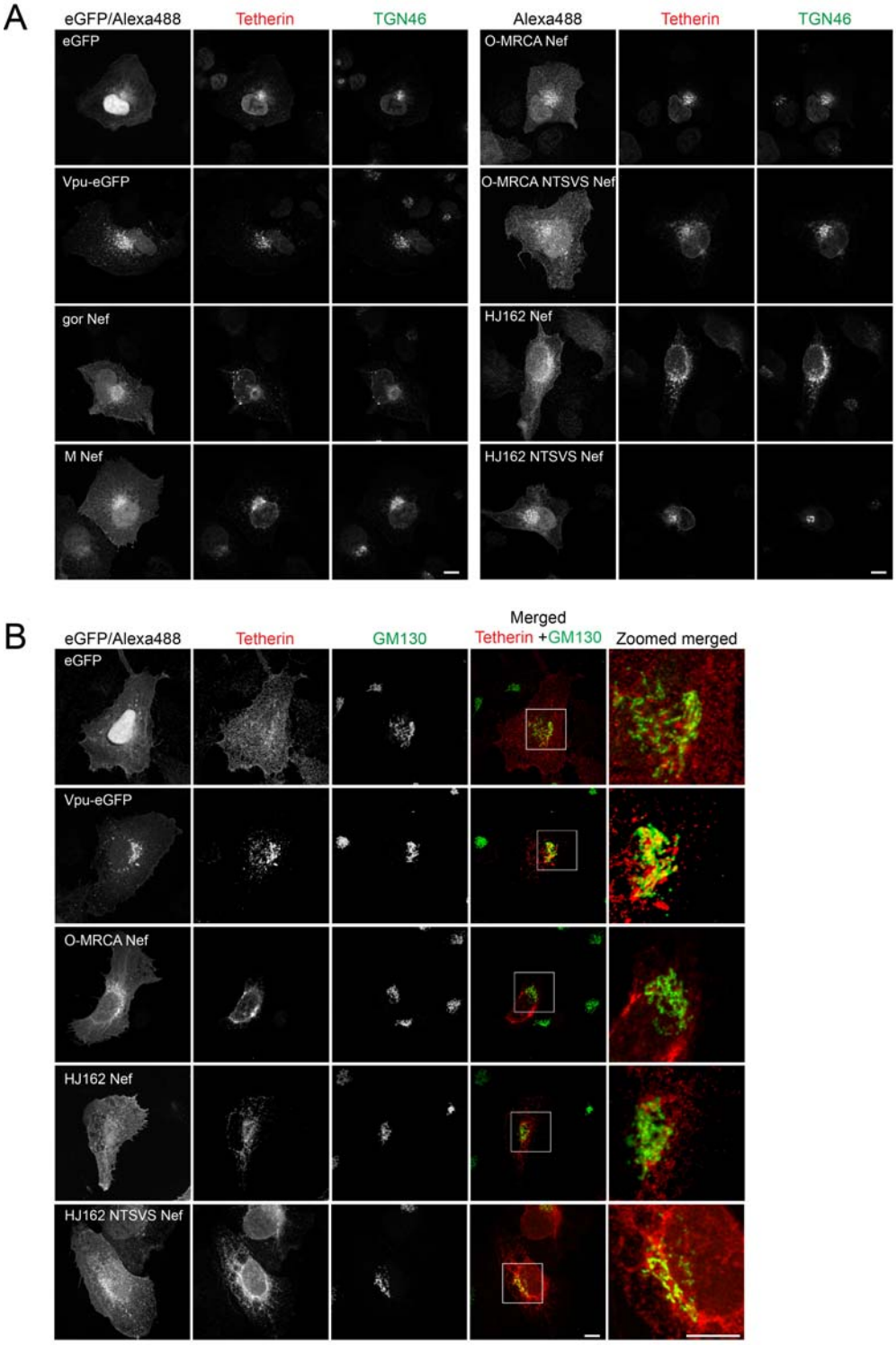

Figure S6 (related to Figure 6). O-Nefs trap human tetherin in the TGN during anterograde transport. Effect of O-Nefs on co-localization of newly synthesized HUM tetherin with subcellular markers. Shown are representative confocal microphotographs of HT1080 cells co-microinjected with a HUM tetherin expression plasmid together with vectors encoding eGFP, or NL4-3 Vpu or the indicated Nef proteins. 2 hours post microinjection, the cells were analyzed for co-localization with markers for the *trans*-Golgi network (TGN46) (A) and the Golgi (GM130) (B). (A) Images of the individual channels for Vpu/Nef, HUM-tetherin and TGN46 of the merged pictures shown in Fig. 5D in black and white. (B) Images of the individual channels for Vpu/Nef, HUM-tetherin and GM130 as well as an overview and zoom of the merged tetherin and marker channels. Scale bar = 10µM.

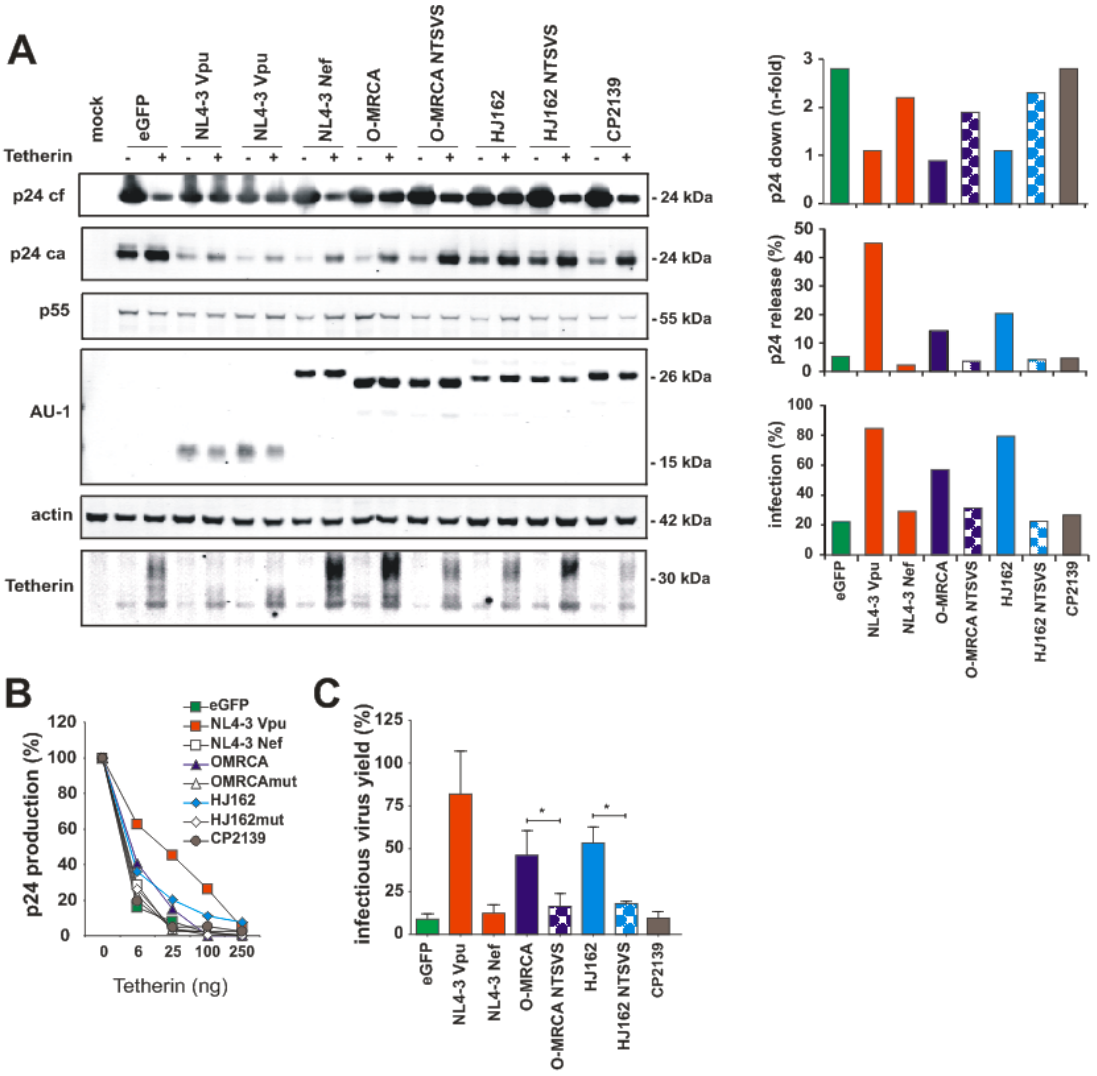

Figure S7 (related to Figure 7). Functional relevance of downmodulation of human tetherin by O-Nefs. (A) Western blot analysis of HIV-1 particle release. 293T cells were cotransfected with a vpu and nef defective HIV-1 NL4-3 proviral construct, with vectors expressing the indicated Nef proteins or Vpu and a plasmid expressing HUM tetherin or an empty control vector. Cell supernatants (cf) and cellular lysates (ca) were probed with an anti-capsid monoclonal antibody. Mock transfected cells were used as negative control; ß-actin was analyzed as a loading control and eGFP to check transfection efficiencies. The levels of HUM tetherin expression differ because Vpu degrades and O-MRCA stabilizes this restriction factor. The right panel shows the reduction of p24 release in the presence of tetherin (upper) and the total levels of p24 antigen determined by ELISA (middle) and the quantity of infectious HIV-1 (lower) in the cell-free culture supernatants of the experiment shown in panel A. The control NL4-3 Vpu was included twice. (B) Effect of O-MRCA and HJ162 wt and mutant Nefs on virus release. 293T cells were cotransfected with a ΔVpuΔNef proviral HIV-1 NL4-3 construct, Nef expression vectors and different quantities of a construct expressing HUM tetherin. The levels of p24 antigen in the culture supernatant were determined by ELISA. (C) Average levels (n=3) of infectious virus release (±SD) in the presence of 25 ng of the HUM tetherin expression construct. (D) Effect of wt and mutant O-Nef proteins on tetherin-induced NF-κB activation. Activation of NF-κB-dependent firefly luciferase reporter gene expression in 293T cells was determined as described in the legend to Figure 3. The results show mean values ±SD of three independent transfections.

Supplemental Experimental Procedures

Generation of MRCA sequences. To estimate the MRCA sequences for HIV-1 groups M, O, and N Nef sequences, phylogenetic trees were constructed for the region extending from the gp41 segment of *env* to the end of *nef* (HXB2 coordinates for group M, 7767-9405; for group O, 7764-9408; and for group N, 7764-9405) sequences respectively. Regions that could not be unambiguously aligned were excluded for calculation of the evolutionary model and phylogenetic tree reconstruction, but were included in MRCA sequence reconstruction. Trees were calculated using MrBayes vers. 3 (Ronquist and Huelsenbeck 2003) based on nucleotide sequences (with a GTR model with gamma-distributed site-to-site rate variation and allowing for invariable sites) and inferred amino acid sequences (mixed model). Analyses were calculated until analysis chains converged adequately (based on an average standard deviation of split frequencies was ≤ 0.01) and a 25% burn-in interval was discarded. The >50% clade credibility topologies from these analyses were used to reconstruct ancestral states. For each tree topology, two different evolutionary models were calculated: 1) the best fit model of nucleotide evolution using the AIC with Modeltest version 3.7 (Posada and Crandall 1998, Posada and Buckley 2004); and 2) the codon model using codeml of PAML version 4.2 (Yang 2007). For the nucleotide evolutionary model, PAUP* (Swofford 1999) was used to reconstruct the nucleotide sequence at ancestral nodes under the likelihood criterion. For the codon model, codeml from the PAML package was used to reconstruct the ancestral codons. Nucleotide sequences from both approaches were then translated to obtain ancestral amino acid sequences. To reconstruct the MRCA amino acid sequences over gapped regions of the alignment, MacClade version 4.08 (Maddison and Maddison 2001) was used to visually reconstruct a maximum parsimony reconstruction based on the MrBayes 50% clade credibility topology.

For most sites in the alignments for MRCA sequence inference, all methods of ancestral state reconstruction were in agreement and predicted the same amino acid. At the remaining sites where the predictions differed, the codon model sequence residue and the protein sequence-inferred tree was used. For sites where no codon model residue prediction was available, or the predictions were equivocal or in disagreement, either the nucleotide model prediction was used if available or visual, parsimony-based predictions using MacClade to predict the residue. The site in the M MRCA that was equivocal in their reconstructions are indicated in Figure S2. The residues chosen to be synthesized at these equivocal sites were chosen based on the most-parsimonious reconstruction by visual inspection of the phylogenies.

Expression vectors. Bi-cistronic CMV promoter-based pCG expression vectors coexpressing *vpu*, *nef*, CD4 or tetherin and the enhanced green fluorescent protein (eGFP) or DsRed2, respectively have been described previously (Sauter et al., 2009). Splice-overlap-extension PCR with primers introducing *XbaI* and *MluI* restriction sites flanking the reading frames was used to generate chimeric *nef* alleles and *nef* mutants. PCR fragments were purified from agarose gels and inserted into the pCG vector using standard cloning techniques. All PCR-derived inserts were sequenced to confirm that no undesired nucleotide changes were present.

Cell culture and transfections. 293T cells were maintained in Dulbecco's modified Eagle medium (DMEM) supplemented with 10% FCS plus 2 mM glutamine and antibiotics and transfected by the calcium phosphate method as described previously (Munch et al., 2007). TZM-bl cells were kindly provided by Drs. Kappes and Wu and Tranzyme Inc. through the NIH AIDS Reagent Program and were kept in DMEM supplemented with 10% FCS plus 2 mM glutamine and antibiotics. TZM-bl cells express large amounts of CD4, CCR5 and CXCR4 and contain the β-galactosidase gene under the control of the HIV-1 promoter (Derdeyn et al., 2000; Platt et al., 1998; Wei et al., 2002). PBMCs from healthy human donors were isolated using lymphocyte separation medium (Biocoll separating solution; Biochrom), stimulated for 3 days with phytohemagglutinin (PHA) (1 µg/ml), and cultured in RPMI-1640 medium with 10% fetal calf serum (FCS) plus 2 mM glutamine, antibiotics and 10 ng/ml interleukin 2 (IL-2) prior to infection.

Flow cytometric analysis. To determine the effect of Vpu and Nef on tetherin and CD4 cell surface expression, either 293T cells were transfected with constructs expressing tetherin, Vpu or Nef, or PBMCs were transduced with *vpu*-deficient NL4-3 constructs expressing different Nefs. 293T cells were transfected by the calcium phosphate method with 1 µg of a tetherin or CD4 expression vector coexpressing eGFP and 5 µg of pCGCG eGFP/Vpu or constructs expressing eGFP alone or together with Vpu or Nef. Two days post-transfection tetherin or CD4 expression was examined by FACS (Schindler et al., 2003). PHA-activated PBMCs were transduced with VSV-G pseudotyped *vpu*-defective HIV-1 NL4-3 constructs expressing the indicated *nef* alleles and examined for tetherin, CD4, MHC-I or Ii surface expression 3 days later. For staining of tetherin or CD4 allophycocyanin-conjugated anti-tetherin (Biolegend, 348410) or anti-human CD4 antibodies (Invitrogen; MHCD0405) were used. For staining of MHC-I or CD74, PE-conjugated anti-human HLA-ABC (Dako; M073601-2) or CD74 (Ancell; 226-050) antibodies were used. Fluorescence of stained cells was detected by two-color flow cytometry and Vpu- or Nef-mediated tetherin, CD4 or MHC-I downmodulation and CD74 upmodulation was calculated as described previously (Kirchhoff et al., 2004; Schindler et al., 2003). Briefly, the mean fluorescence intensities were determined for cells showing specific ranges of eGFP expression. The fluorescence values obtained for cells transfected with the control construct expressing only eGFP was compared with the corresponding number obtained for cells coexpressing Vpu or Nef.

Tetherin antagonism. To determine the capability of Vpu and Nef to antagonize tetherin, 293T cells were seeded in six-well plates and transfected with 4 µg of NL4-3 Δ*vpu* IRES eGFP, 1 µg Vpu or Nef expression plasmid and different amounts of tetherin expression vectors (6 well). At two days post-transfection supernatants were harvested and the yield of infectious HIV-1 was determined by a 96-well infection assay on TZM-bl indicator cells as described previously (Munch et al., 2007). The p24 antigen concentrations were quantified by using an HIV-1 home-made p24 capture ELISA or by Western Blot.

Western Blot. To monitor Vpu and Nef expression, 293T cells were transfected with 5 µg of vector DNA coexpressing eGFP and AU1 tagged Vpus or Nefs. Two days post-transfection cells were harvested, lysed in M-PER buffer (ThermoScientific) containing a protease inhibitor cocktail (Roche) and cell lysates were separated in 4-12% Bis-Tris gels (Invitrogen). After gel electrophoresis, proteins were transferred onto PVDF membranes and probed with an AU1 antibody (Covance, MMS-130P). Subsequently, blots were probed with anti-mouse or anti-rabbit IRDye Odyssey antibodies (926-32210, 926-32221) and proteins detected using a LI-COR Odyssey scanner. For internal controls, blots were incubated with antibodies specific for eGFP (290-50, Abcam) and β-actin (8227-50, Abcam).

Immunofluorescence staining and confocal microscopy. HEK293T cells were seeded 24 h before transfection at a density of 20,000 cells per well on a 8-well ibidi slides (80826, ibidi GmbH, Germany) which was freshly coated with poly-L-lysine. When cells were about 60-70% confluent, they were transfected with 150 ng of AU1 tagged Nef, 50 ng of hu-Tetherin-HA and 50 ng of pAcGFP1-Mem (GFP-Mem, 632491, Clontech) expression plasmids using Lipofectamine 2000 Transfection Reagent (11668-019, Life Technologies). At 16 hours post-transfection, live cell were stained with 1:500 dilution of mouse anti-HA antibody (Tetherin) for 30 min. Cells were then immediately fixed with 4% cold PFA for 15 min. After washing with PBS, cells were permeabilized and stained with 1:500 dilutions of mouse anti-HA and rabbit anti-AU1 antibodies (both Covance) in a solution of 0.2 % saponin, 0.25% fish skin gelatin (Sigma) and 0.2% BSA in PBS. After 1 hour, cells were thoroughly washed with PBS and incubated with Alexa Flour-568 and -647 conjugated secondary antibodies targeting primary antibodies (all antibodies at 1:500 dilution; life technologies) for 2 h. Finally, cells were washed thoroughly and kept in PBS. Images were taken on a LSM710 confocal microscope (Carl Zeiss, Germany) equipped with Plan-Apochromat 63x/1.40 oil objective lenses and Zeiss Zen 2010 software. GFP-Mem was excited using a 488 nm laser and Alexa Flour-568 and -647 dyes were excited by 561 nm and 633 nm lasers, respectively. Respective emissions were collected using appropriate beam splitters. Further analysis was performed with the latest version of FIJI software (http://fiji.sc/wiki/index.php/Fiji). Data was normalized in Excel software (Microsoft Inc.) and plotted using GraphPad Prism.

Tetherin anterograde biosynthetic transport assay. HT1080 cells grown on coverslips were microinjected into their nuclei with an AIS 2 microinjection apparatus using pulled borosilicate glass capillaries in principle as reported (Schmidt et al., 2011). Constructs encoding an HA-tagged HU-tetherin and plasmids encoding eGFP, AU1 tagged Vpu or different Nefs variants were mixed in water at concentrations of 5 ng/µl each, and co-injected. Following microinjection, cells were cultured for 1, 2 or 6 hours at 37°C to allow protein expression and trafficking. At the indicated time points cells were fixed with 4% paraformaldehyde/PBS, permeabilized, and HU-tetherin molecules were detected using a mouse anti-HA-tag antibody (Santa Cruz Biotechnology) followed by a goat anti-mouse Alexa-568 secondary antibody (Invitrogen). Newly synthesized Nef molecules fused to AU1 were detected using rabbit anti-AU1 (Covance) and anti-rabbit Alexa-488 secondary antibody (Invitrogen). For co-localization analysis, cells were fixed and permeabilized 2 hours post microinjection and stained for Nef as described above, HA-tagged HU-tetherin using a chicken anti-HA antibody (Abcam), and an antibody against subcellular markers (Golgi: mouse anti GM130 (BD); TGN: sheep anti TGN46; early endosomes: goat anti EEA1 (Santa Cruz); ER: rabbit anti-calreticulin (Stressmarq Biosciences inc)) followed by staining with the appropriate secondary antibodies. Stained cells were imaged with a Leica SP5 confocal microscope except the images for co-localization with subcellular markers that were acquired on PerkinElmer UltraVIEW VoX spinning disc microscope equipped with a Hamamatsu ORCA Flash4.0 V2 camera and a 60x Apo TIRF 1.49 Oil objectif.

Endocytosis assay. 293T cells were cotransfected with a tetherin vector and Vpu or Nef expressing IRES eGFP constructs. 48 h post transfection, surface tetherin was stained using an unconjugated anti-tetherin antibody (ebioscience, 16-3179-82) and an APC-conjugated secondary anti-mouse antibody (Invitrogen, A865) at 4°C. Endocytosis was allowed for up to 30 mins at 37°C and samples were taken at the indicated time points. Samples were split in two halves. One set was washed for 50 sec with DMEM pH2, the other half was left untreated. Cells were fixed and after FACS analysis of the tetherin-APC signal of eGFP positive cells, endocytozed proportion was determined by dividing intracellular by total MFI.

IFNα sensitivity assay. CD4+ T-cells were positively selected (Miltenyi Biotec) from buffy coats of healthy donors (Research Blood Components) and activated using beads loaded with biotinylated antibodies against human CD2, CD3 and CD28 (Miltenyi Biotec) for 4 days. Activated CD4+ T-cells were divided and one half treated with 500U/ml IFNα2 (PBL Laboratories) for 24 hours. The following day, cells were resuspended at 5x106 per ml in media (15% RPMI containing 30U/ml IL-2) and incubated overnight with equivalent amounts of each virus (2ng RT activity of 293T-derived virus stocks). Cells were washed three times with 1ml of PBS and cultured in media (either containing IFNα2 or not). 100µl of media was sampled with replacement (including IFNα2 where appropriate) every 48 hours. At day 5, cells and supernatants were harvested to quantify p24 antigen. Cells were lysed in 1x Triton-X-containing buffer for 1 hour at 37ºC and lysates were clarified by centrifugation. Supernatants and cell lysates were used to quantify particle- associated/ cell-free and cell- associated

p24 respectively by a high sensitivity alphaLISA (Perkin Elmer). The percentage of cell-free p24 divided by total (cell-free plus cell-associated) p24 was calculated in the presence and absence of IFNα2. These experiments were performed in triplicate in CD4+ T-cells derived from three healthy donors.

Supplemental References

Charneau, P., Mirambeau, G., Roux, P., Paulous, S., Buc, H., and Clavel, F. (1994). HIV-1 reverse transcription. A termination step at the center of the genome. J. Mol. Biol. 241, 651–662.

Derdeyn, C.A., Decker, J.M., Sfakianos, J.N., Wu, X., O'Brien, W.A., Ratner, L., Kappes, J.C., Shaw, G.M., and Hunter, E. (2000). Sensitivity of human immunodeficiency virus type 1 to the fusion inhibitor T-20 is modulated by coreceptor specificity defined by the V3 loop of gp120. J. Virol. 74, 8358–8367.

Maddison, W.P., and Maddison, D.R. (2001). MacClade - Analysis of Phylogeny and Character Evolution - Version 4 (Sunderland, MA: Sinauer Associates, Inc.).

Münch, J., Rajan, D., Schindler, M., Specht, A., Rücker, E., Novembre, F.J., Nerrienet, E., Müller-Trutwin, M.C., Peeters, M., Hahn, B.H., et al. (2007). Nef-mediated enhancement of virion infectivity and stimulation of viral replication are fundamental properties of primate lentiviruses. J. Virol. *81*, 13852–13864.

Platt, E.J., Wehrly, K., Kuhmann, S.E., Chesebro, B., and Kabat, D. (1998). Effects of CCR5 and CD4 cell surface concentrations on infections by macrophage-tropic isolates of human immunodeficiency virus type 1. J. Virol. 72, 2855–2864.

Posada, D., and Buckley, T. (2004). Model selection and model averaging in phylogenetics: advantages of akaike information criterion and bayesian approaches over likelihood ratio tests. Syst Biol 53, 793-808.

Posada, D., and Crandall, K.A. (1998). MODELTEST: testing the model of DNA substitution. Bioinformatics 14, 817-818.

Ronquist, F., and Huelsenbeck, J.P. (2003). MrBayes 3: Bayesian phylogenetic inference under mixed models. Bioinformatics 19, 1572-1574.

Schindler, M., Würfl, S., Benaroch, P., Greenough, T.C., Daniels, R., Easterbrook, P., Brenner, M., Münch, J., and Kirchhoff, F. (2003). Down-modulation of mature major histocompatibility complex class II and up-regulation of invariant chain cell surface expression are well-conserved functions of human and simian immunodeficiency virus nef alleles. J. Virol 77, 10548–10556.

Swofford, D.L. (1999). PAUP* 4.0: Phylogenetic Analysis Using Parsimony (*and Other Methods) (Sunderland, MA: Sinauer Associates, Inc.).

Wei, X., Decker, J.M., Liu, H., Zhang, Z., Arani, R.B., Kilby, J.M., Saag, M.S., Wu, X., Shaw, G.M., and Kappes, J.C. (2002). Emergence of resistant HIV-1 in patients receiving fusion inhibitor (T-20) monotherapy. Antimicrob. Agents Chemother. 46, 1896–1905.

Yang, Z. (1997). PAML: a program package for phylogenetic analysis by maximum likelihood. Comput Appl Biosci 13, 555-556.

Yang, Z. (2007). PAML 4: phylogenetic analysis by maximum likelihood. Mol Biol Evol 24, 1586-1591.